MOVING FINITE ELEMENT MODELLING OF COMPRESSIBLE FLOW

M.J. BAINES AND A.J. WATHEN

NUMERICAL ANALYSIS REPORT 4/85

The work reported here forms part of the research programme of the Oxford/Reading Institute for Computational Fluid Dynamics and was funded by the R.A.E., Farnborough under contract no. ER1/9/4/2035/054XR/Aero.

MOVING FINITE ELEMENT MODELLING OF COMPRESSIBLE FLOW

M.J. Baines and A.J. Wathen

1. INTRODUCTION

Increases in computer power, and considerable improvements in numerical methodology have been significant features in the advance of computational aerodynamics in recent years. In particular, these advances have made possible more widespread simulation of complicated high speed compressible flows. Further development of numerical methodology has been stimulated by the desire for flexible and efficient algorithms, and this has been reflected in the continuing research into methods which in some way adapt to the flow field. The work of this report forms part of this research effort.

Finite difference methods are well advanced in the numerical modelling of compressible flows but finite element methods, despite their flexibility and capacity for reproducing important physical properties, have yet to establish themselves as strong competitors in the field. Nevertheless important work is being carried out by a number of workers[1,2,3], based on Galerkin, Petrov-Galerkin and Characteristic Galerkin methods which may change the balance.

One of the difficulties is the representation of shocks. In the standard finite element approach the nodal values are not the approximate values of the variable represented but rather the whole finite element approximation has the character of a best fit to the solution. As a result shocks appear with oscillations in the finite element approximation and the exact position of the shock has to be recovered by a fitting process. Although this phenomenon is also present to some extent in finite difference methods it is more local,

and with the sophisticated techniques now available the effect is minimised and acceptable.

An important result which deserves wider attention is that of Herbst[4] who has shown that for linear finite element solutions of the Burgers equation

$$u_t + uu_x = \varepsilon u_{xx} \tag{1.1}$$

which possess a shock structure with a jump J and satisfy Neumann boundary conditions, v_x satisfies

$$\varepsilon \sum v_x^2 = \frac{J^3}{12} \quad . \tag{1.2}$$

As ε decreases the sum increases and, on any predetermined grid, v must eventually oscillate to satisfy (1.2). Regarding hyperbolic equations as limits of such parabolic equations as $\varepsilon \to 0$, the difficulties of representing shocks on fixed grids by finite element methods become obvious.

Adaptive grid methods have recently gained attention as ways of introducing extra flexibility into fixed grid methods. In finite differences the work of Berger[5] and Flaherty[6] and in finite elements that of Miller[7,8] and Lohner[9] are important contributions. The invention by Miller of the Moving Finite Element (MFE) method which determines a finite element approximation with moving nodes as a single system, has produced notable results for parabolic problems but, owing to technical difficulties, has not progressed as quickly as it might have done ,(but see Moser, Djomehri).

These technical difficulties have now largely been overcome by Wathen[10], and the resulting MFE method has proved to be very efficient and accurate for the solution of simple scalar conservation laws in one space dimension. Initial computations for hyperbolic problems in 2 space dimension (Wathen (1984)) have also shown how the method is able to sharply model moving shocks, for hyperbolic problems. The clear need has been to develop experience and understanding of the various ways in which the ideas inherent in the method can be extended for application to systems of equations, particularly the system of gas dynamic equations.

The work of this contract has been to describe and assess the various approaches. As a starting point we have used the Euler equation in 1-dimension as a test-bed, and analysed the performance of two different extensions of the MFE scalar algorithm on the bursting membrane problem used by Sod (1978). As was to have been expected, various previously unforeseen features arose in both approaches. These are described, and remedies proposed in the appropriate sections of this report.

The layout of the paper is as follows. After a brief description of the original MFE development of Miller we describe a novel viewpoint which clarifies the issues and shows the power of the method for scalar hyperbolic conservation laws. The issues arising in the extension of the method to systems of equations are discussed and first results given for the application of the method to the Sod shocktube problem [13]. Finally a discussion is given of the advantages and limitations of the method.

2. BASIC METHOD

We begin with a short summary of the MFE method as developed by Miller and others[14]. We confine ourselves to one dimension and initially to hyperbolic conservation laws of the form

$$u_t + f_x = 0 \quad , \tag{2.1}$$

and describe both the basic method and some recent results which bring out the local nature of the method.

In the MFE description the object function u is replaced by a continuous piecewise linear spline with moving nodes. This approximation v may be written

$$v(x,t) = \sum_{j=0}^{N+1} a_j(t)\alpha_j(x,\underline{s}(t)) \quad , \tag{2.2}$$

where the α_j are time dependent basis functions, ones which take the value 1 at a (moving) node and zero at all other nodes (see Fig. 2.1). The a_j are the nodal coefficients (heights) and the s_j (formed into a vector $\underline{s}$) are the nodal co-ordinates.

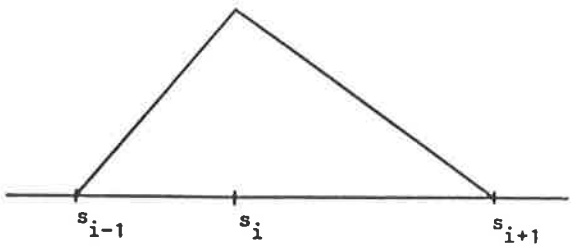

Figure 2.1
Basis function α_i

Assuming fixed boundaries, differentiation of v with respect to time gives

$$v_t = \dot{a}_0\dot{\alpha}_0 + \sum_{j=1}^{N} [\dot{a}_j\alpha_j + \dot{s}_j\beta_j] + \dot{a}_{N+1}\alpha_{N+1} \tag{2.3}$$

(dropping dependence and using a dot for the time differentiation). The results of Lynch[15] show that the function β_j is given by

$$\beta_j = - v_x\alpha_j \tag{2.4}$$

and is a second-type basis function which has the same support as α_j

but is discontinuous at s_j. It is also solution-dependent through v_x in (2.4).

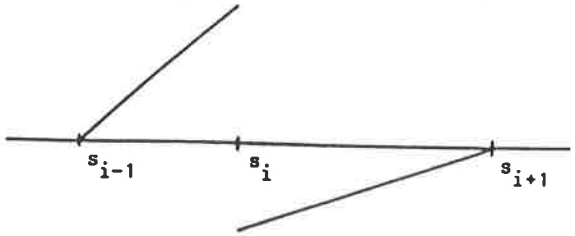

Figure 2.2
Basis function β_i

To obtain $\dot{a}_j$ and $\dot{s}_j$ (and hence the evolution of the approximation (2.2)), Miller minimises the residual

$$\| v_t + f(v)_x \|_2 \tag{2.5}$$

in the L_2 norm over the $\dot{a}_j$ and $\dot{s}_j$. This gives the (semi-discrete) MFE equations in the form

$$\langle \alpha_j, v_t + f(v)_x \rangle = 0 \qquad (j = 0,\ldots,N+1) \tag{2.6}$$

$$\langle \beta_j, v_t + f(v)_x \rangle = 0 \qquad (j = 1,\ldots,N). \tag{2.7}$$

Note that equations (2.6) are the Galerkin equations for (2.1) and, since the α_j are a partition of unity, conservation is incorporated. Combining (2.6) and (2.7) into a single system we obtain

$$A(\underline{y})\dot{\underline{y}} = \underline{g} \tag{2.8}$$

where

$$\underline{y} = \{a_0; a_1, s_1; \ldots; a_N, s_N; a_{N+1}\} \ , \tag{2.9}$$

$A(\underline{y})$ is a 2x2 block tridiagonal matrix (apart from boundary effects) with blocks

$$\begin{bmatrix} \langle \alpha_j, \alpha_j \rangle & \langle \alpha_j, \beta_j \rangle \\ \langle \beta_j, \alpha_j \rangle & \langle \beta_j, \beta_j \rangle \end{bmatrix} \tag{2.10}$$

and the corresponding block of $\underline{g}$ is

$$\underline{g}_j = \begin{bmatrix} \langle \alpha_j, -f(v)_x \rangle \\ \langle \beta_j, -f(v)_x \rangle \end{bmatrix} . \qquad (2.11)$$

Since A is singular if the nodes become collinear (parallelism) or if nodes overtake Miller adds penalty functions to (2.5) to prevent these singularities occurring. This modifies the ODE system (2.8) so that it becomes stiff. He therefore uses a stiff solver to carry out the time stepping for $\underline{y}$ and hence v.

It has been shown by Wathen and Baines[16] that the matrix A possesses the decomposition

$$A = M^T C M \qquad (2.12)$$

where both M and C are 2x2 block diagonal matrices (though with the blocks of M staggered with respect to the blocks of C). As a result A is trivially invertible and there are only two sources of singularity of A, namely that of M and that of C. Singularity of M corresponds to collinearity of nodes (parallelism) and is easily circumvented without recourse to penalty functions (see below). Singularity of C corresponds to node overtaking. This is modelled as the formation of a shock (see below) and again penalty functions are unnecessary.

Moreover it has also been shown[16] that, if D is the matrix of diagonal blocks of A, the preconditioning of A by D^{-1} gives a matrix $D^{-1}A$ which has eigenvalues $\pm\frac{1}{2}$ only (apart from boundary effects). All this means that A is easily invertible by for example conjugate gradient methods and the ODE system (2.8) does not need a stiff solver.

An alternative viewpoint is to replace the set of basis functions α_0, α_j, β_j $(j = 1,2,\ldots,N+1)$ α_{N+1} by the half-hat functions ϕ_{k1}, ϕ_{k2} $(k = 1,2,\ldots,N+1)$ (see Fig. 2.3). The set $\{\phi_{k1}, \phi_{k2}\}$ span the same space as the set $\{\alpha_j, \beta_j\}$

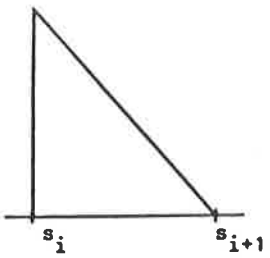

Basis function ϕ_{k1}

Figure 2.3

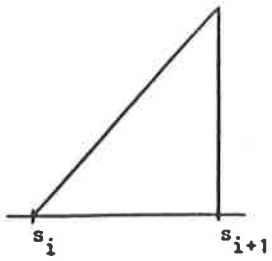

Basis function ϕ_{k2}

so that (2.6), (2.7) may be replaced by

$$\langle \phi_{k1},\ v_t + f(v)_x \rangle = 0 \qquad (2.13)$$

$$\langle \phi_{k2},\ v_t + f(v)_x \rangle = 0 \qquad (2.14)$$

and, if we write

$$v_t = \sum_{k=1}^{N} [\dot{w}_{k1}\phi_{k1} + \dot{w}_{k2}\phi_{k2}] \qquad (2.15)$$

(c.f. (2.3)), we obtain the alternative MFE equations

$$C\underline{\dot{w}} = \underline{b} \quad , \qquad (2.16)$$

where

$$\underline{\dot{w}} = \{\dot{w}_{11},\dot{w}_{12};\dot{w}_{21},\dot{w}_{22};\ldots;\dot{w}_{N+1,1},\dot{w}_{N+1,2}\} \quad , \qquad (2.17)$$

C is the 2x2 block diagonal matrix with blocks

$$\begin{bmatrix} \langle \phi_{k1},\phi_{k1} \rangle & \langle \phi_{k1},\phi_{k2} \rangle \\ \langle \phi_{k2},\phi_{k1} \rangle & \langle \phi_{k2},\phi_{k2} \rangle \end{bmatrix} \qquad (2.18)$$

and the corresponding block of $\underline{b}$ is

$$\underline{b}_k = \begin{bmatrix} \langle \phi_{k1},\ -f(v)_x \rangle \\ \langle \phi_{k2},\ -f(v)_x \rangle \end{bmatrix} \quad . \qquad (2.19)$$

From the connection between the ϕ's and the α,β's (see Fig. (2.3)) we also have

$$M\dot{\underline{y}} = \underline{\dot{w}} \quad , \qquad (2.20)$$

where (apart from boundary effects) M is the 2x2 block diagonal matrix with blocks

$$\begin{bmatrix} 1 & -\mu_{j-\frac{1}{2}} \\ 1 & -\mu_{j+\frac{1}{2}} \end{bmatrix} \quad , \tag{2.21}$$

μ being v_x and $j-\frac{1}{2}$, $j+\frac{1}{2}$ referring to the elements on either side of the node j. The relation to the Miller approach with $A = M^T C M$ is completed by noting that

$$\underline{g} = M^T \underline{b} \quad . \tag{2.22}$$

Equations (2.13) and (2.14) are the normal equations for the L_2 projection of $f(v)_x$ into the space spanned by the ϕ_{k1}, ϕ_{k2}. The result is the best linear fit in L_2 to the function $f(v)_x$ in the element k. Since this is identified with v_t we have at any instant that v_t is the best <u>local</u> fit to $f(v)_x$ within the element k.

Once $\dot{\underline{w}}$ is known $\dot{\underline{y}}$ is determined from equation (2.20). If the nodes to the left and the right of the kth element are j and $j+1$, we have

$$\left.\begin{aligned} \dot{a}_j - \mu_k \dot{s}_j &= \dot{w}_{k1} \\ \dot{a}_{j+1} - \mu_k \dot{s}_{j+1} &= \dot{w}_{k2} \quad . \end{aligned}\right\} \tag{2.23}$$

Subtraction and division by $\Delta s = s_{j+1} - s_j$ gives

$$\frac{d\mu_k}{dt} = \frac{1}{\Delta s} (\dot{w}_{k2} - \dot{w}_{k1}) \tag{2.24}$$

where

$$\mu_k = (a_{j+1} - a_j)/(s_{j+1} - s_j) \tag{2.25}$$

is the slope of the solution. To obtain the right hand side, we note that $[-1,1]$ is an eigenvector of C with eigenvalue $\frac{1}{6}\Delta s$ so that

$$(\dot{w}_{k2} - \dot{w}_{k1}) = [-1,1]^T \underline{b}_k = \langle \phi_{k2} - \phi_{k1}, -f(v)_x \rangle \quad , \tag{2.26}$$

which gives

$$\frac{d\mu_k}{dt} = \frac{6}{(\Delta s)^2} \int_{s_j}^{s_{j+1}} (\phi_{k2} - \phi_{k1}) f(v)_x \, dx \quad . \tag{2.27}$$

This can be written

$$\frac{d\mu_k}{dt} = \frac{12}{(\Delta s)^2} \{\bar{f} - \hat{f}\} \tag{2.28}$$

where

$$\bar{f} = \tfrac{1}{2}(f_j + f_{j+1}), \quad \hat{f} = \frac{1}{\Delta s}\int_{s_j}^{s_{j+1}} f(v)\, dx \ . \tag{2.29}$$

Equation (2.28) shows how the slope μ_k depends on the flux function f. In particular it shows how μ_k increases or decreases depending on the convexity of f.

The revised viewpoint above brings out the local nature of the method. The movement of each node is generated by a local projection of the flux function of the approximation in adjacent elements.

Time stepping is carried out on the semi-discrete equations (2.8) or (2.20) with (2.17). Such is the well-behavedness of the system that there is no need to use other than explicit Euler forward time stepping of the form

$$\underline{y}^{n+1} - \underline{y}^n = \Delta t M^{-1} \underline{\dot{w}}^n \ . \tag{2.30}$$

[Note that $\underline{\dot{w}}^n$ is determined from (2.16) and the time stepping is only in (2.20)].

The method breaks down if either C of (2.17) or M of (2.20) is singular. Singularity of M corresponds to parallelism of nodes. There is then an infinity of solutions of the system (2.20) as a result of blocks (2.21) being singular. Uniqueness is easily restored by imposing an external condition which suitably sets the position of the parallel nodes[10,16].

Singularity of C corresponds to one node overtaking the next as in Fig. 2.4. In that case we cannot determine the projection of $f(v)_x$ into the (null) element. Instead we regonise the event as indicating the occurrence of a shock. Support for this view is given by a result of Morton[17] who showed that in the present case the MFE equations carry the best L_2 fit to the solution.

In place of the two missing equations of (2.16) or (2.8) we use the Rankine-Hugoniot shock relations

$$\dot{s}_j = \dot{s}_{j+1} = \left(\frac{f_{j+1} - f_j}{a_{j+1} - a_j}\right) \qquad (= V) \tag{2.31}$$

where V is the shock speed. The effect is to partition the region into two regions in each of which the method is applied, the connection across being made by the internal boundary condition (2.31).

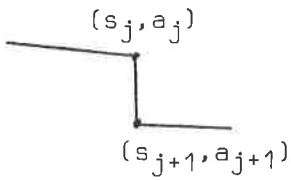

Figure 2.4

When a node runs into a shock it is absorbed by the shock in that (2.31) is used to recalculate the shock speed V while one node is able to be deleted. The time step can be chosen to be as large as the shortest time for any two nodes to become coincident. In general, however, accuracy will determine a lower time step.

This, then, is the complete algorithm for a scalar hyperbolic conservation law in one dimension. Results are shown in Section 3 for two simple equations, (1.1) with $\varepsilon = 0$ and the Buckley-Leverett equation.

$$u_t + \left(\frac{u^2}{u^2 + \frac{1}{2}(1-u)^2}\right)_x = 0 \quad . \tag{2.32}$$

The corresponding MFE algorithm for higher dimensions incorporates the same essential ideas of shock recognition and the avoidance of degeneracy using algebraic considerations. A full description is given in Wathen & Baines (1985) and Wathen (1984). From this latter reference, we reproduce the results of two dimensional computation of the MFE solution of the hyperbolic conservation law

$$\frac{\partial u}{\partial t} + \nabla \cdot \left(\frac{u^2}{u^2 + \frac{1}{2}(1-u)^2}\right) = 0$$

which arises in the modelling of hydrocarbon reservoir flows (Figure 3).

We continue the paper by discussing the extension to systems of conservation laws with particular reference to the Euler equations in one space dimension.

3.1 EXTENSION TO SYSTEMS

In extending the above ideas to systems the most important question to be answered is whether (A) to work with separate nodal coefficients but a common mesh or (B) to give each component of the system its own finite element mesh with individual model coefficients and co-ordinates.

Where discontinuous features are likely to occur simultaneously for all components, as in the case of shocks, there is a strong argument for using a common mesh. However, a nicer algebraic structure is obtained if each component is given its own finite element mesh. We shall briefly describe both possible strategies, called method (A) and method (B) respectively.

In method (A) we seek continuous piecewise linear finite element approximations

$$\rho(x,t) = \sum_{j=0}^{N+1} \rho_j(t)\, \alpha_j(x,\underline{s}(t)) \tag{3.1}$$

$$m(x,t) = \sum_{J=0}^{n+1} m_j(t)\, \alpha_j(x,\underline{s}(t)) \tag{3.2}$$

$$e(x,t) = \sum_{j=0}^{N+1} e_j(t)\, \alpha_j(x,\underline{s}(t)) \tag{3.3}$$

to functions ρ, m, e (density, momentum and energy) on the single mesh

$$\underline{s}(t) = \{s_0(t), s_1(t), \ldots, s_{N+1}(t)\}^T \quad . \tag{3.4}$$

The evolution of ρ_j, s_j is then determined by solving the density equation ((2.1) with $u = \rho$, $f(u) = m$) using the MFE method as described for the scalar equation. We have chosen the density as the variable which determines the nodal movement, rather than any other choice, because it is the experience of many workers that the density is the most sensitive quantity in many compressible

flow situations. J.H.B. Smith[19] of RAE has, however, indicated to us that for certain flows, the density may not be an appropriate choice. The example of a jet flow into an orthogonal free stream highlights this point. With the understanding that there may be some single variable which satisfies our desired criteria, we continue to describe method A with, for definiteness, the density as this variable.

We minimise the L_2 norm of the density equation

$$\| \rho_t + m_x \|_{L_2} \tag{3.5}$$

over $\dot{\rho}_j$ and $\dot{s}_j$ where

$$\rho_t = \dot{\rho}_0 \alpha_0 + \sum_{j=1}^{N} [\dot{\rho}_j \alpha_j + \dot{s}_j \beta_j^{\rho}] + \dot{\rho}_{N+1} \alpha_{N+1} \tag{3.6}$$

and

$$\beta_j^{\rho} = - \rho_x \alpha_j \ . \tag{3.7}$$

We have assumed fixed boundaries s_0, s_{N+1} but allowed variable states ρ_0 and ρ_{N+1} as in Section 2. Other boundary conditions can be incorporated when necessary[10]. The corresponding MFE semi-discrete equations are

$$\langle \alpha_j, \rho_t + m_x \rangle = 0 \qquad (j = 0,1,\ldots,N+1) \tag{3.8}$$

$$\langle \beta_j^{\rho}, \rho_t + m_x \rangle = 0 \qquad (j = 1,2,\ldots,N) \tag{3.9}$$

which can be written as the matrix system (2.8) or (2.17) plus (2.20) and solved for $\dot{\rho}_j$, $\dot{s}_j$ $\forall_j$.

Now time differentiation of (3.2) and (3.3) gives

$$m_t = \dot{m}_0 \alpha_0 + \sum_{j=1}^{N} [\dot{m}_j \alpha_j + \dot{s}_j \beta_j^{m}] + \dot{m}_{N+1} \alpha_{N+1} \tag{3.10}$$

$$e_t = \dot{e}_0 \alpha_0 + \sum_{j=1}^{N} [\dot{e}_j \alpha_j + \dot{s}_j \beta_j^{e}] + \dot{e}_{N+1} \alpha_{N+1} \tag{3.11}$$

and since $\dot{s}$ is known the only unknowns in these expressions are $\dot{m}_j$ and

$\dot{e}_j$. Writing the Euler momentum and density equations as

$$m_t + f^m_x = 0, \qquad e_t + f^e_x = 0 \tag{3.12}$$

we obtain Galerkin equations on the mesh with the already found velocity $\dot{s}_j$, namely,

$$\left.\begin{aligned} \langle \alpha_j,\ m_t + f^m_x \rangle &= 0 \qquad (3.13)\\ \langle \alpha_j,\ e_t + f^e_x \rangle &= 0 \qquad (3.14) \end{aligned}\right\} \quad i = 0,1,\ldots,N+1$$

for the $\dot{m}_j$ and $\dot{e}_j$. These equations are not MFE equations in the sense of Section 2 and the resulting matrix forms do not have the simple structure described there.

The shock algorithm needs special consideration. Suppose that, after a time step, a pair of nodes coincide. The resultant internal boundary (shock or contact discontinuity) thus formed is subsequently moved at the speed V given by the appropriate shock relation

$$V = \frac{m_{j+1} - m_j}{\rho_{j+1} - \rho_j} \quad . \tag{3.15}$$

As the states ρ_j, ρ_{j+1} and m_j, m_{j+1} which form the shock vary so will the speed of the discontinuity.

The evaluation of the inner products in (3.13), (3.14) deserves some comment. Consider the integral $\langle \alpha_j,\ f^m_x \rangle$ which involves integrals of the form

$$\int_{s_i}^{s_{i+1}} \alpha_j \frac{\partial}{\partial x}\left(\frac{m^2}{\rho}\right) dx \quad , \tag{3.16}$$

where $m = m_j + (m_{j+1}-m_j)x$ and $\rho = \rho_j + (\rho_{j+1}-\rho_j)x$ are linear on the element between the nodes j, $j+1$. Evaluation of (3.16) when $\rho_{j+1} \neq \rho_j$ yields

$$\tfrac{1}{2}\frac{(m_{j+1} - m_j)^2}{(\rho_{j+1} - \rho_j)} - a + \frac{b}{(\rho_{j+1} - \rho_j)} \log(\rho_{j+1}/\rho_j) \tag{3.17}$$

where

$$a = \left(\frac{m_{j+1} - m_j}{\rho_{j+1} - \rho_j}\right)^2 \rho_j - 2\,\frac{(m_{j+1} - m_j)}{\rho_{j+1} - \rho_j}\, m_j \qquad (3.18)$$

and

$$b = m_j^2 + a\rho_j = \left\{m_j - \left(\frac{m_{j+1} - m_j}{\rho_{j+1} - \rho_j}\right)\rho_j\right\}^2 . \qquad (3.19)$$

For $\rho_{j+1} = \rho_j$, the value of the integral (3.16) is however

$$\frac{1}{\rho_j}\left\{\frac{1}{3}(m_{j+1} - m_j)^2 + m_j(m_{j+1} - m_j) + m_j^2\right\} \qquad (3.20)$$

and it is seen that only by cancellation of large terms in the formula (3.17) is the limit (3.20) achieved when $\rho_{j+1} - \rho_j \to 0$. As noted previously by Djomehri[12] this causes computational problems, and we have followed his work in expanding the denominator in (3.16) (3.17) in a binominal series for small values of $\rho_{j+1} - \rho_j$. A similar technique is used for terms me/ρ and m^3/ρ^2 which arise in the energy equation.

Method (B) seeks continuous piecewise linear finite element approximations

$$u^{(\ell)}(x,t) = \sum u_j^{(\ell)}(t)\alpha_j^{(\ell)}(x,\underline{s}^{(\ell)}(t)) \qquad (\ell=1,2,3) \quad (3.21)$$

where $u^{(1)} = \rho$, $u^{(2)} = m$, $u^{(3)} = e$. The whole of Section 2 is now applicable, the only complications being the evaluation of the integrals (2.11) or (2.19), and the shock algorithm. With regard to shocks, the difficulty here is that because of inaccuracies in the numerical method, the shocks do not (quite) happen simultaneously. Nevertheless in the knowledge that such features which nearly occur together should indeed occur together, a strategy can be invented which overcomes the difficulty.

With regard to the evaluation of the integrals (2.11), we note that this is the only point in this exposition at which we must consider the construction of multidimensional algorithms which include conceptual differences from procedures previously described and used in 1-D.

The procedure that we use though not seemingly the most efficient in one dimension, is in fact immediately applicable to 2 and 3-D. The more obvious one-dimensional algorithm would be to construct the 'global grid' which is the set of all node points of all variables. A simple ordering of these in the single direction would then leave sub-element line segments on which all variables are linear, and the necessary integral evaluations could easily be performed. The generalisation of this in, for example, 2-D where we use triangular grids for each components, would however introduce arbitrary polygonal sub-elements over which to perform the integrations. The alternative algorithm that we have actually employed is to directly apply a quadrature formula for each element of the mesh of each particular component. We then need only to find the value of other components at the appropriate integration points. Because we are employing a finite element representation, these values are easily found without the need for interpolation.

We now consider application of the two methods to the well-known Sod shocktube problem [13]. The lack of an exact or approximate Riemann solver in the MFE method at present causes immediate difficulty in moving away from the initial discontinuous state. In fact the value of MFE methods in aerodynamics is likely to be in computing flows which evolve from smooth initial data to develop discontinuities. The shocktube problem run from the initial state is thus a stern test. We have therefore used an exact Riemann solver made available by Sweby to give the solution at a non-zero time t_0, and used that data as initial conditions for the MFE method.

The results are given in Section 4. Firstly we describe the results of method (A). The shock and contact are modelled extremely accurately but it was noticed that nodes in the rarefaction wave moved leftwards and upwards in such a way that there was good resolution of the upper part of the rarefaction but no resolution towards the bottom part. If the program was run for sufficient time nodes in the rarefaction wave moved to the top of the wave and merged with the node already there. That is, coincidence of nodal coefficients and co-ordinates occurred in the sense that

$$s_j \to s_{j-1}, \qquad \rho_j \to \rho_{j-1} \tag{3.22}$$

simultaneously.

This feature may be explained analytically by considering equations (3.8), (3.9). Since the term m_x is piecewise constant on the mesh $\underline{s}$ it lies in the space in which ρ_t is sought. Thus no projection is required and there is an exact solution of the equation

$$\rho_t + m_x = 0 \quad .$$

This leads to the results (c.f. (2.24) or (2.28))

$$\frac{d\mu_k^\rho}{dt} = 0 \qquad \mu_k^\rho = \text{const.} \tag{3.23}$$

$$\dot{\rho}_j = \frac{(m_j/\rho_j)^R - (m_j/\rho_j)^L}{\rho_j^R - \rho_j^L} \qquad \dot{s}_j = \frac{m_j^R - m_j^L}{\rho_j^R - \rho_j^L} \tag{3.24}$$

for each k, j. We therefore see that, for all elements k, the slope μ_k is constant in time, and that, for all nodes j in the rarefaction wave, $\dot{a}_j > 0$ and $\dot{s}_j < 0$ regardless of nodal separation. Thus nodes move leftwards and upwards and merge at the top of the rarefaction, which means that resolution of the rarefaction is lost.

This difficulty is seen in Figure 4, where we have taken $t_0 = 0.10$. We present the results in Figure 5 of an attempt to override this pr oblem. For all nodes i in the rarefaction wave, we have enforced that $\dot{\rho}_i = 0$, by removing the relevant terms in the expansion for ρ_t. For this run we have taken $t_0 = 0.0072$.

For method (B) the above difficulty does not arise because in general the ρ nodes and m nodes will not coincide and the property (3.23) does not follow, allowing more flexibility. The numerical results given in Figure 6 were obtained using 14 nodes on each of the three moving meshes.

4. CONCLUSION

These first results for the present MFE methods as applied to the Sod problem show that if a single moving mesh is used in the MFE solution with piecewise linear approximation resolution in the rarefaction is inevitably lost simply as a result of the nature of the approximation for m. We have tested a method of overcoming this difficulty.

If separate moving meshes are used such problems may not arise, and indeed our our computations using this method appear quite promising.

ACKNOWLEDGEMENTS

We acknowledge useful discussions with J.H.B. Smith and C.C. Lytton of R.A.E., Farnborough and are indebted to Robin Dixon of ICFD at Reading for invaluable help in the programming of these results.

REFERENCES

1. MORTON, K.W. (1984) Generalised Galerkin Methods for Hyperbolic Problems, Report 84/1, Oxford Univ. Computing Lab., England.

2. ZIENKIEWICZ, O.C. (1984) Proceedings of MAFELAP 1984, Brunel University, (to appear).

3. HUGHES, T.J.R. & BROOKS, A.N. (1982) A theoretical framework for Petrov-Galerkin methods with discontinuous weighting functions: applications to the streamline-upwind procedure, in: R.H. Gallagher, D.H. Norrie, J.T. Oden & O.C. Zienkiewicz, eds., Finite Elements in Fluids, Vol. 4, 47-65.

4. HERBST, B.M. (1982) Moving Finite Element Methods for the solution of Evolution Equations. Ph.D. Thesis, University of the Orange Free State.

5. BERGER, M.J. & OLIGER, J. (1984) Adaptive Mesh Refinement for Hyperbolic Partial Differential Equations, J. Comput. Phys., 53, 484.

6. DAVIS, S.F. & FLAHERTY, J.E. (1982) An Adaptive Finite Element Method for Initial-Boundary Value Problems for Partial Differential Equations. SIAM J. Sci. Stat. Comput. 3, 6-27.

7. MILLER, K. & MILLER, R.N. (1981) Moving Finite Elements, Part I. SIAM J. Numer. Anal. 18, 1019-1032.

8. MILLER, K. (1981) Moving Finite Elements, Part II. SIAM J. Numer. Anal. 18, 1033-1057.

9. LOHNER, R., MORGAN, K. & ZIENKIEWICZ, O.C. (1984) An Adaptive Finite Element Method for High Speed Compressible Flow, Institute for Numerical Methods in Engineering Report C/R/479/84, Swansea, U.K.

10. WATHEN, A.J. (1984) Ph.D. Thesis, University of Reading, England.

11. MOSER, C. Application of a Variable Node Finite Element Method to the Gas Dynamics Equns., (1983) in Proc. of 5th GAMM Conf. (Vieweg)(to appear).

12. DJOMEHRI, J. (1983) Ph.D. Thesis, Univ. of California, Berkeley.

13. SOD, G.A. (1978) A Survey of Several Finite Difference Methods for Systems of Nonlinear Hyperbolic Conservation Laws. J. Comput. Phys. 27, 1-31.

14. GELINAS, R.J., DOSS, S.K. & MILLER, K. (1981) The Moving Finite Element Method: Application to General Partial Differential Equations with Multiple Large Gradients. J. Comput. Phys. 40, 202-249.

15. LYNCH, D.R. (1982) Unified Approach to Simulation on Deforming Elements with Application to Phase Change Problems. J. Comput. Phys. 47, 387-411.

16. WATHEN, A.J. & BAINES, M.J. (1983) On the structure of the Moving Finite Element Equations. Num. Anal.Rpt. 5/83, University of Reading. To appear in IMAJ Num. Anal. (1985)

17. MORTON, K.W. (1982) Private communication.

18. SWEBY, P.K. (1984) Private communication.

19. SMITH, J.H.B. (1984) Private communication.

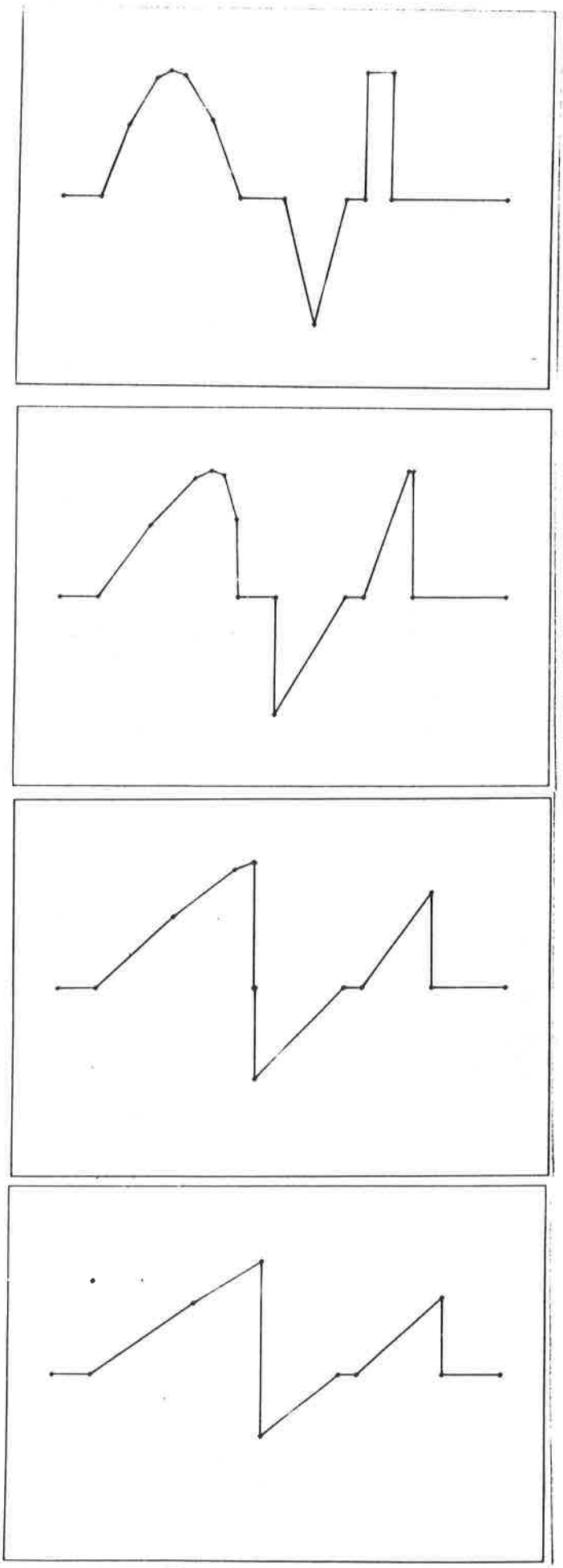

FIGURE 1 Inviscid Burgers Equation : Solution plotted at $t = 0, 0.5, 1.0$ and 1.5 with $\Delta t = 0.1$

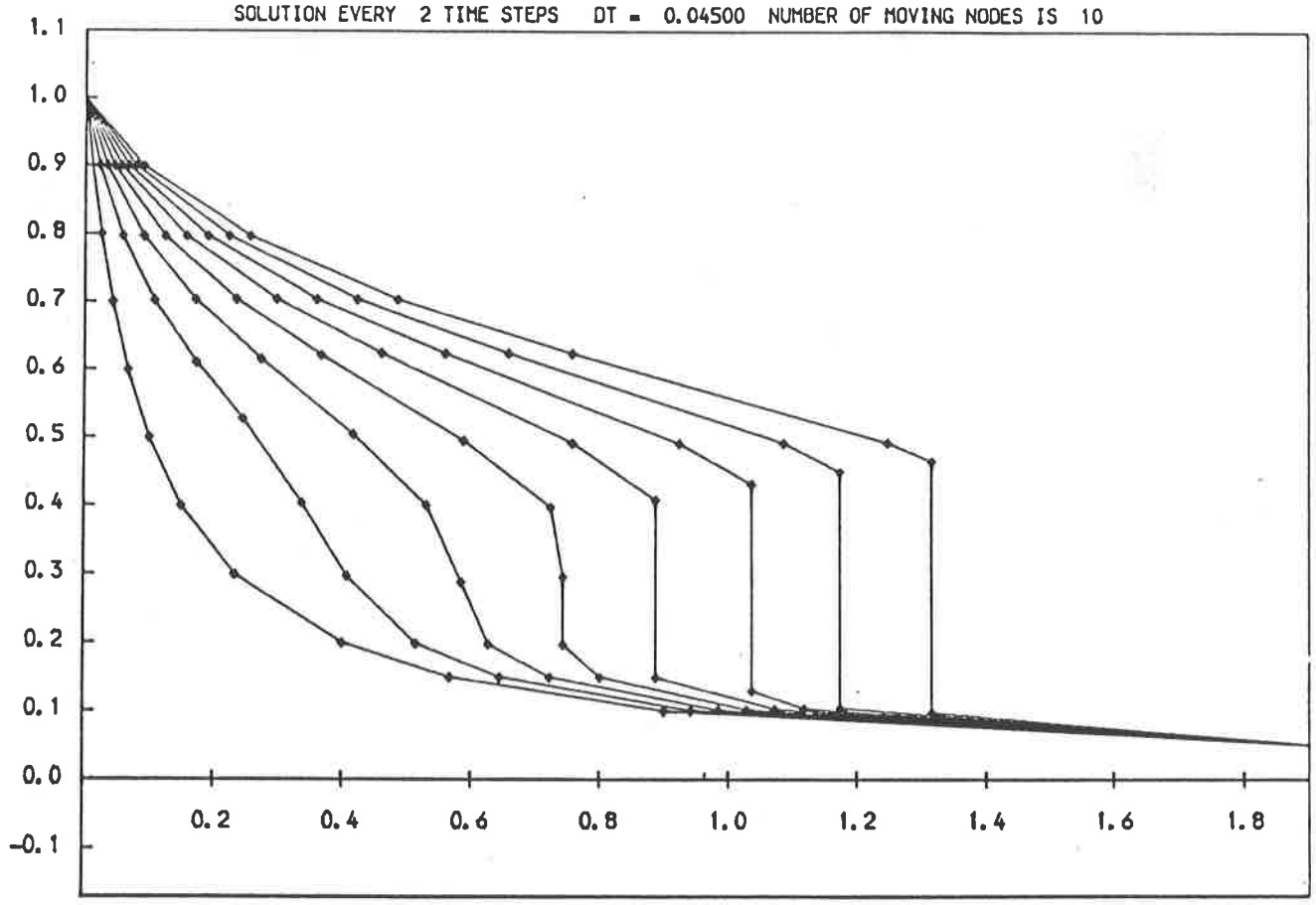

FIGURE 2a Buckley-Leverett Equation : Solution plotted every 2 time-like steps with $\Delta T = 0.045$

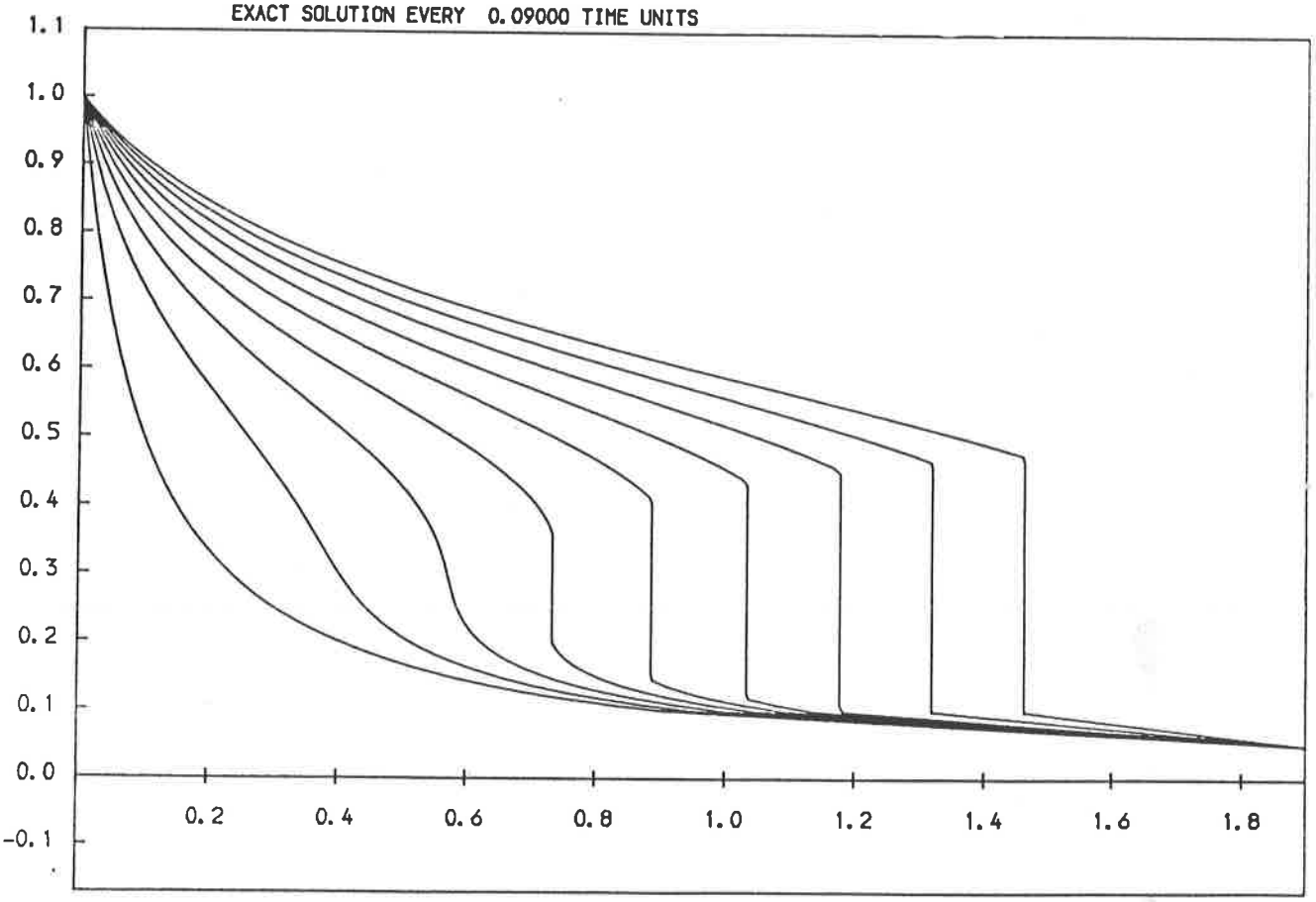

FIGURE 2b Buckley-Leverett Equation : Exact solution every 0.09 time-like units

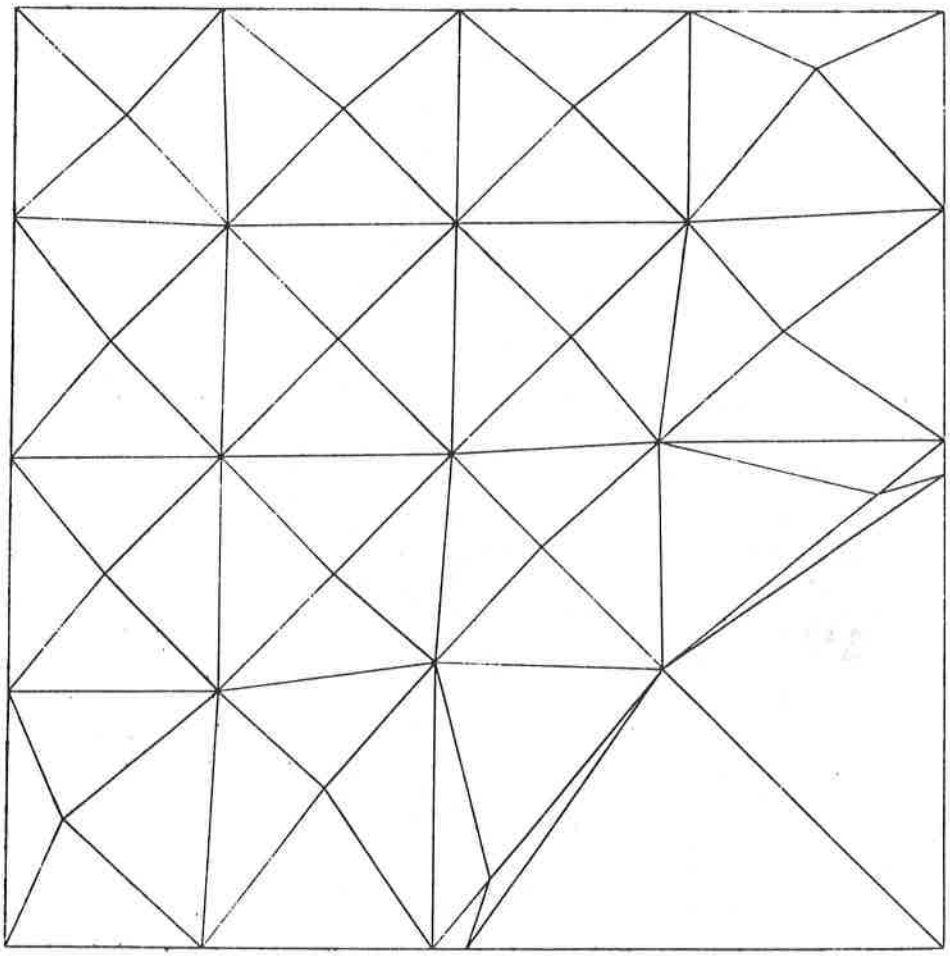

FIGURE 3a Two-dimensional MFE mesh

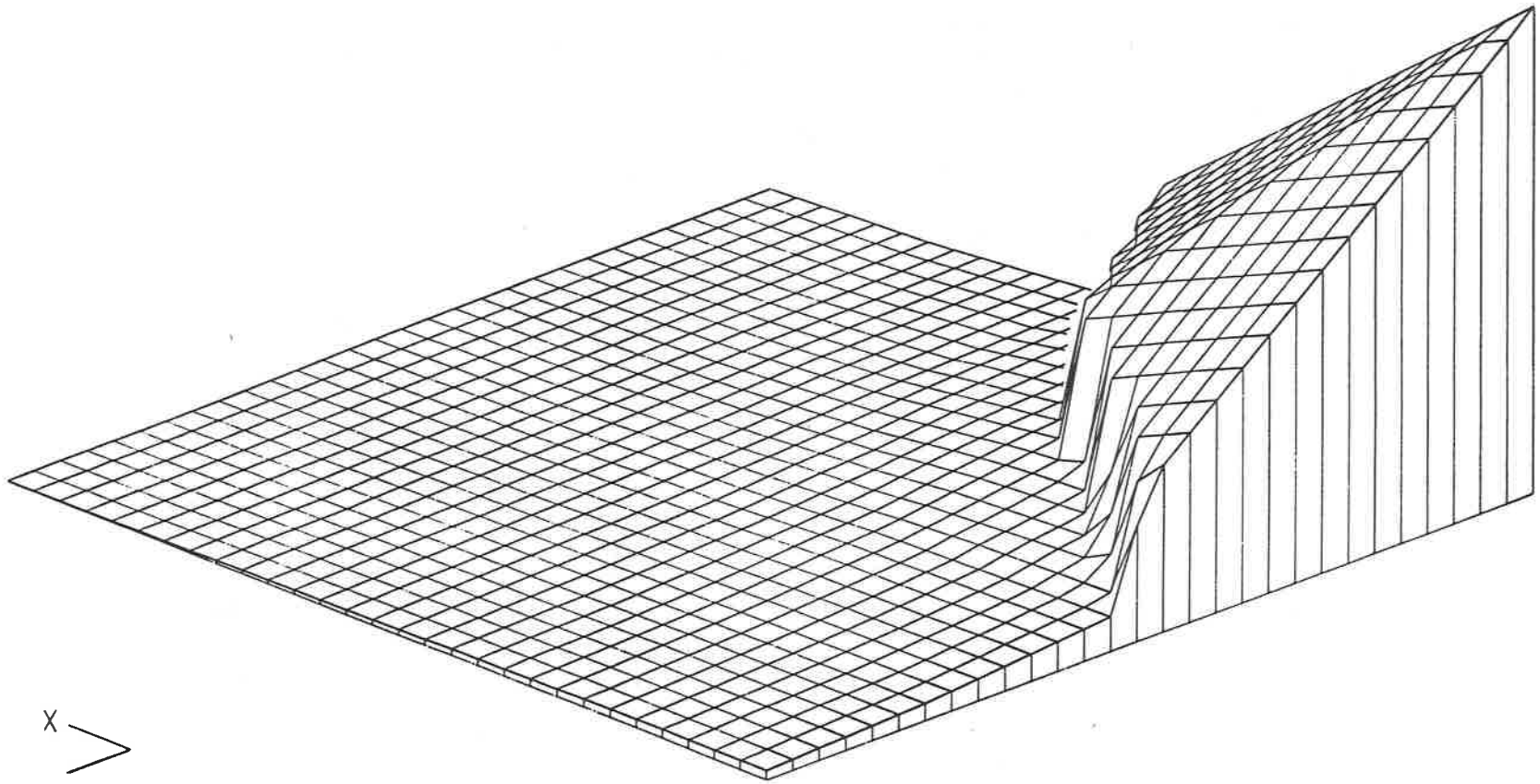

FIGURE 3b Isoplot of MFE solution

SOLUTION AT TIME 0.1000000

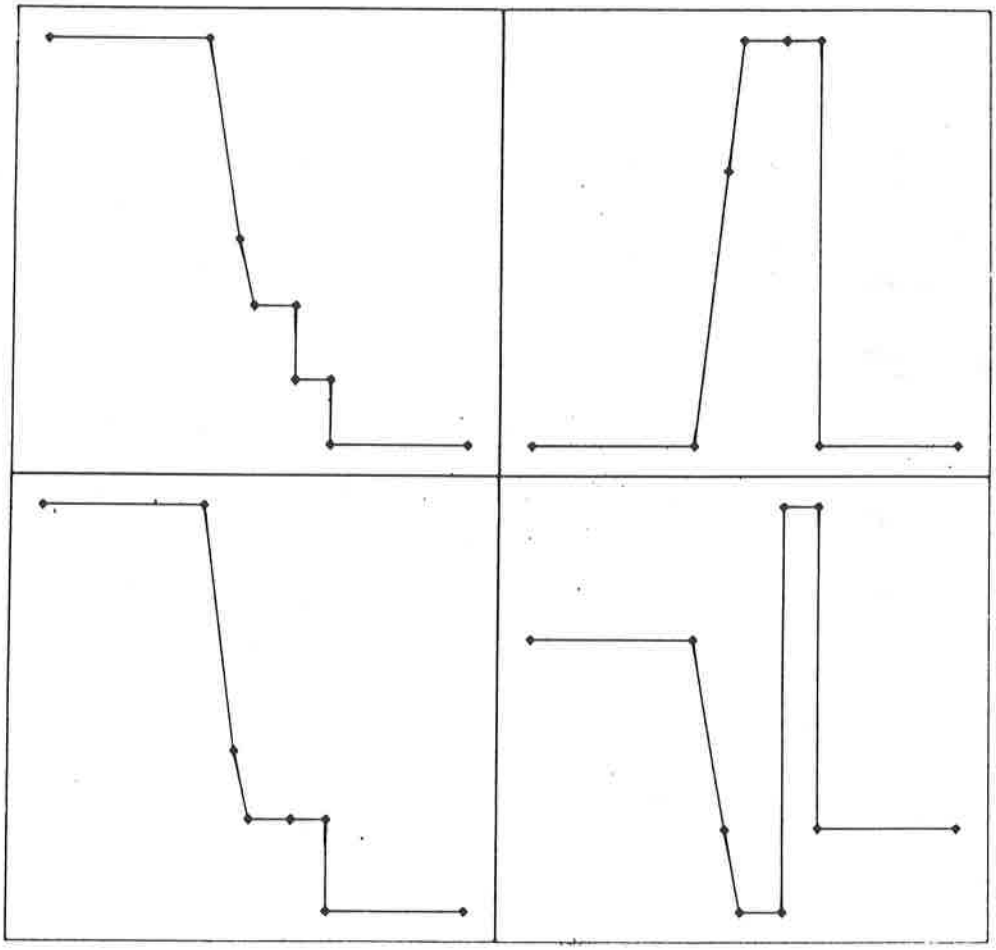

FIGURE 4a

SOLUTION AT TIME 0.1440000

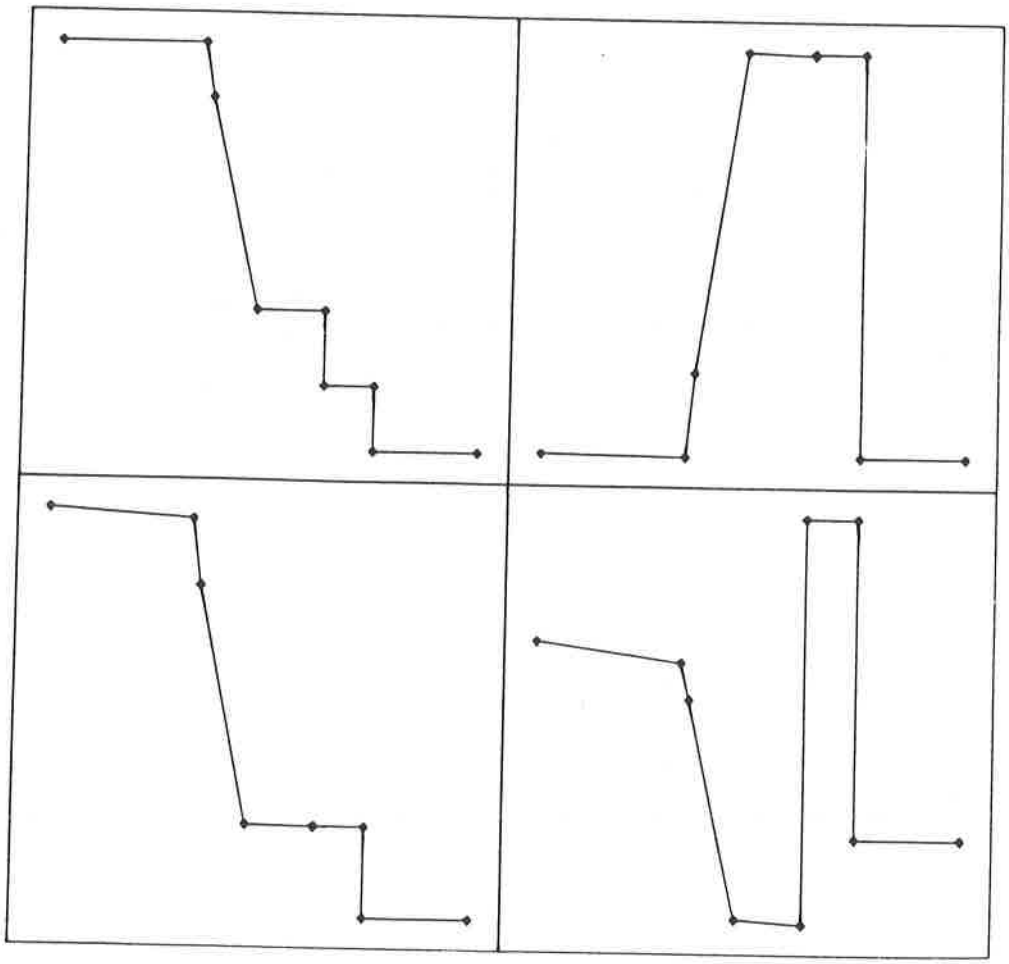

FIGURE 4b

SOLUTION AT TIME 0.0072000

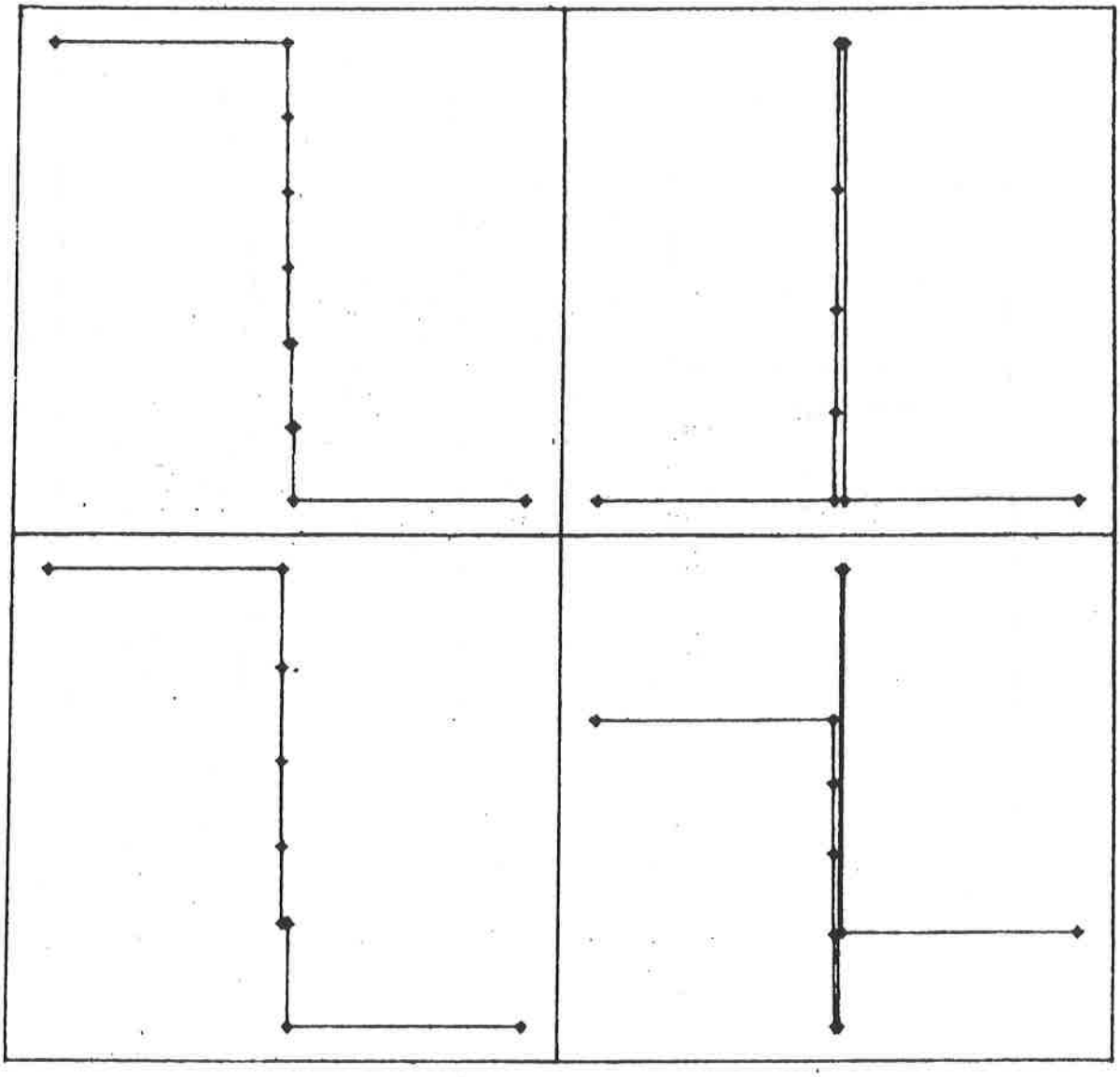

FIGURE 5a

SOLUTION AT TIME 0.1440000

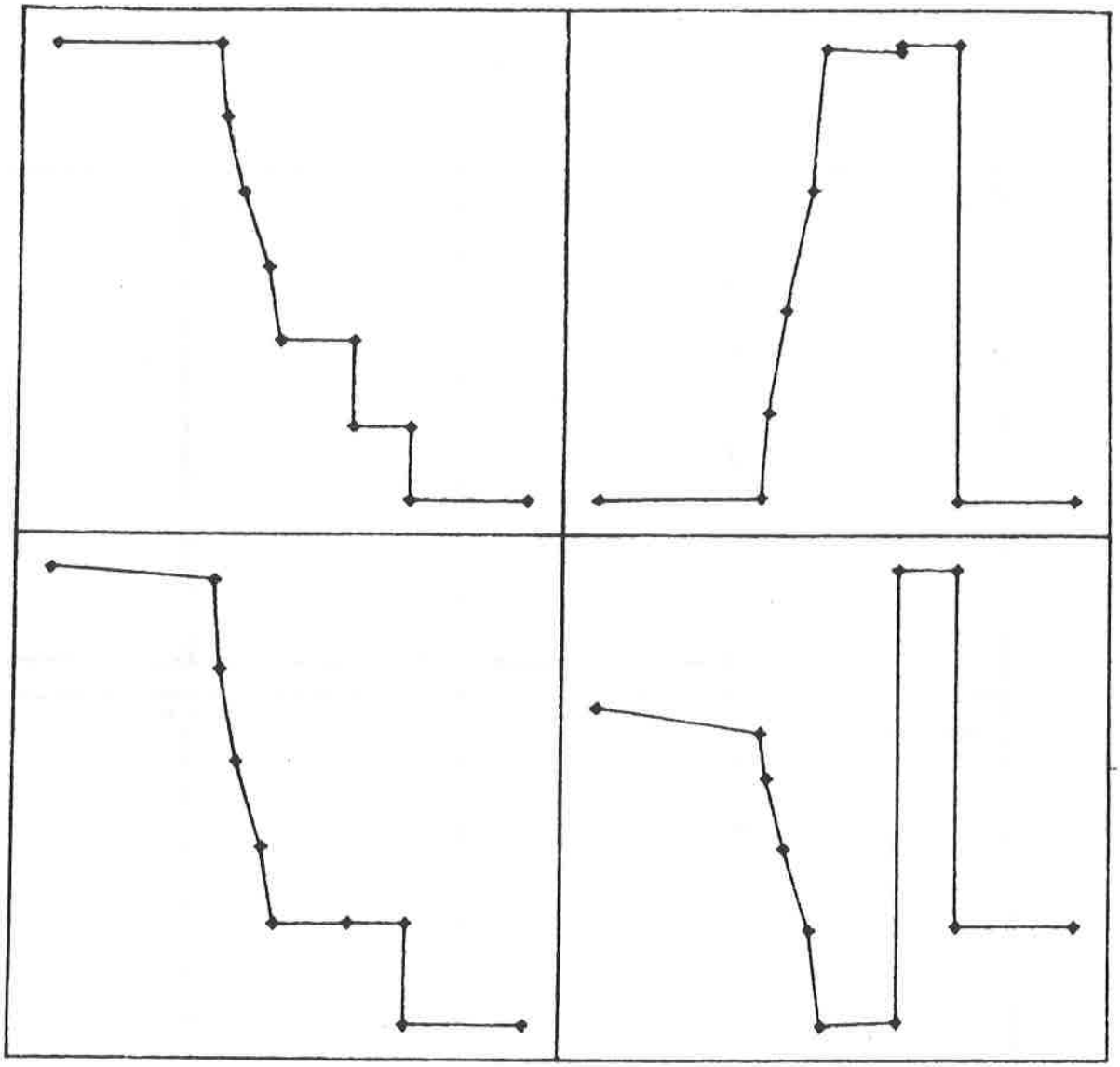

FIGURE 5b

SOLUTION AT TIME 0.1000000

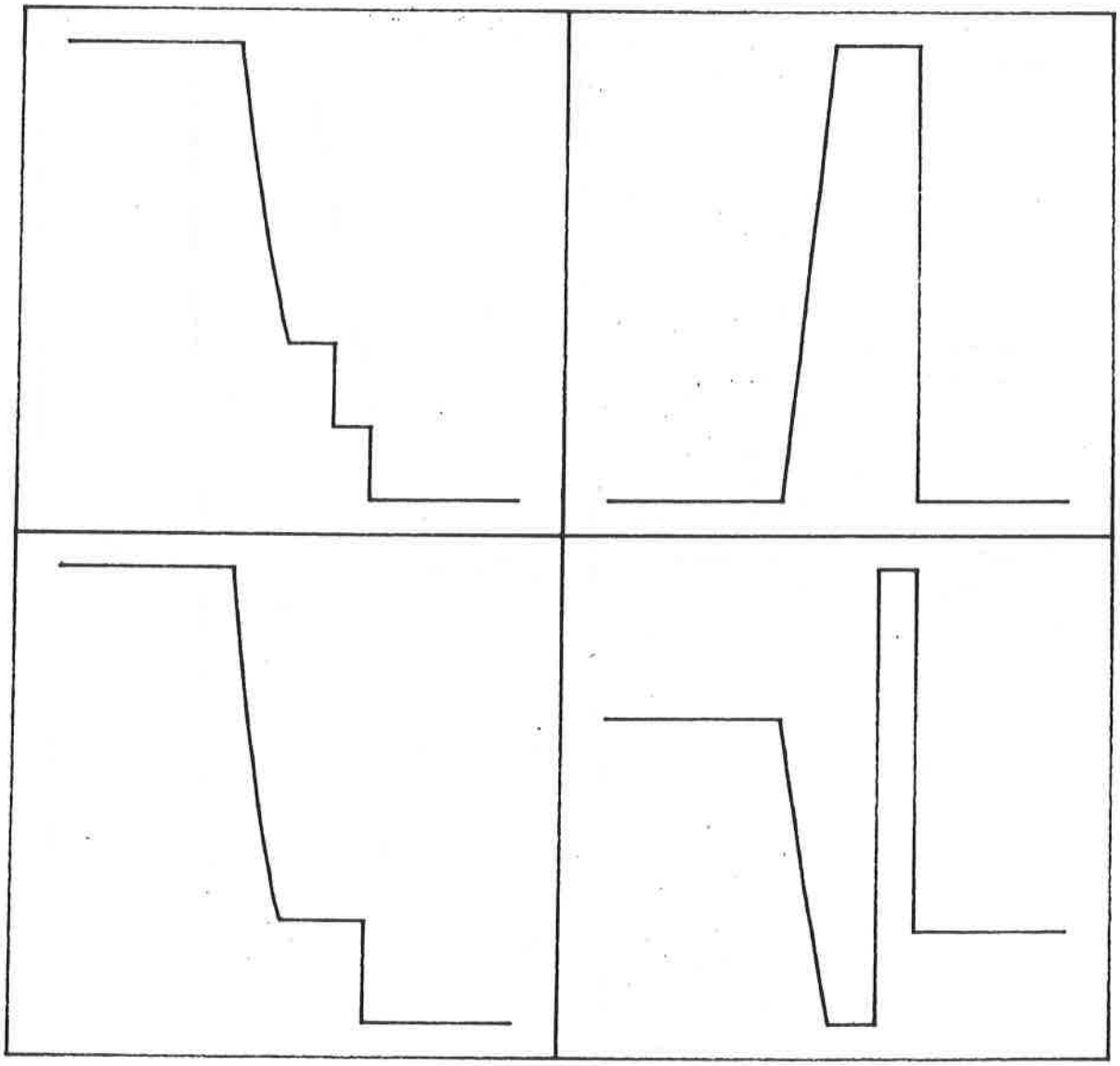

FIGURE 6a

SOLUTION AT TIME 0.1440000

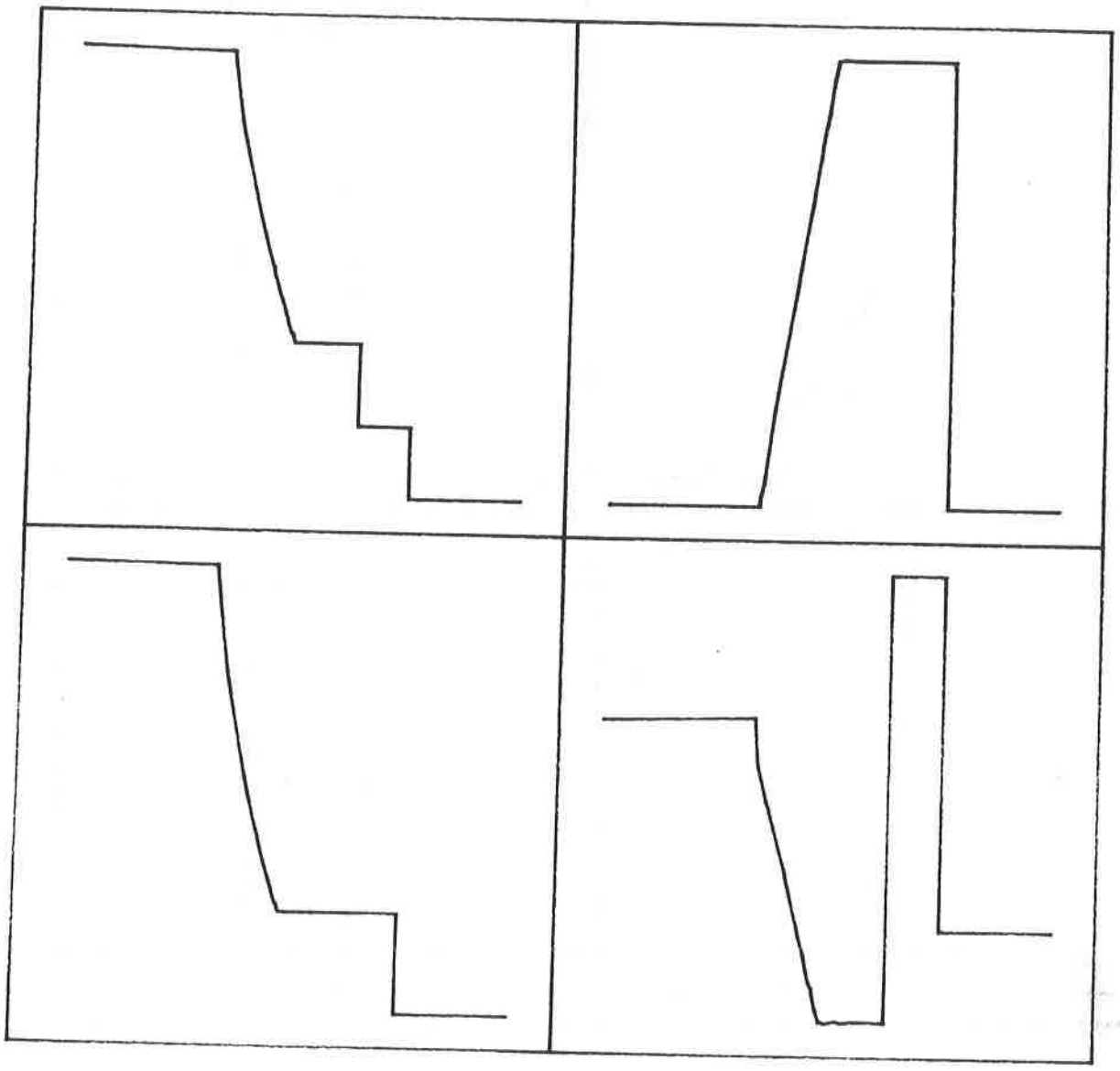

FIGURE 6b